LETTER

doi:10.1038/nature23873

Delta progradation in Greenland driven by increasing glacial mass loss

Mette Bendixen[1]*, Lars Lønsmann Iversen[2]*, Anders Anker Bjørk[3,4,5], Bo Elberling[1], Andreas Westergaard-Nielsen[1], Irina Overeem[6], Katy R. Barnhart[7], Shfaqat Abbas Khan[8], Jason E. Box[9], Jakob Abermann[10], Kirsty Langley[10] & Aart Kroon[1]

Climate changes are pronounced in Arctic regions and increase the vulnerability of the Arctic coastal zone[1]. For example, increases in melting of the Greenland Ice Sheet and reductions in sea ice and permafrost distribution are likely to alter coastal morphodynamics. The deltas of Greenland are largely unaffected by human activity, but increased freshwater runoff and sediment fluxes may increase the size of the deltas, whereas increased wave activity in ice-free periods could reduce their size, with the net impact being unclear until now. Here we show that southwestern Greenland deltas were largely stable from the 1940s to 1980s, but prograded (that is, sediment deposition extended the delta into the sea) in a warming Arctic from the 1980s to 2010s. Our results are based on the areal changes of 121 deltas since the 1940s, assessed using newly discovered aerial photographs and remotely sensed imagery. We find that delta progradation was driven by high freshwater runoff from the Greenland Ice Sheet coinciding with periods of open water. Progradation was controlled by the local initial environmental conditions (that is, accumulated air temperatures above 0 °C per year, freshwater runoff and sea ice in the 1980s) rather than by local changes in these conditions from the 1980s to 2010s at each delta. This is in contrast to a dominantly eroding trend of Arctic sedimentary coasts along the coastal plains of Alaska[2], Siberia[3] and western Canada[4], and to the spatially variable patterns of erosion and accretion along the large deltas of the main rivers in the Arctic[5–7]. Our results improve the understanding of Arctic coastal evolution in a changing climate, and reveal the impacts on coastal areas of increasing ice mass loss and the associated freshwater runoff and lengthening of open-water periods.

With rising global temperatures, Arctic sea-ice extent diminishes[8], and the duration of open water increases, causing severe pressure on the Arctic coastlines[9] through increased wave action[10–12]. Simultaneously, the erodibility of the coast is greatly enhanced by thawing permafrost[5]. Warming also results in increased runoff from the Greenland Ice Sheet and the thousands of peripheral glaciers and ice caps in the Arctic[13,14]. These changes alter the transport of sediment and nutrients from land to the coastal zone[15,16] and can change the morphodynamics of the coastal zone by increasing the fluxes of sediments[17].

Here we undertake a comprehensive investigation of Arctic deltas by mapping the coastal morphodynamic change in 121 Greenlandic deltas from 1940s to 2010s, thereby covering a large spatio-temporal climate gradient in Greenland. These deltas are located between the Greenland Ice Sheet and the ocean, and they act as an effective sedimentary sink before transport to the glacially carved fjords. The fjords, as receiving basins[18], are known as important traps of carbon en route from land to the ocean[19]. Hence, changes in the morphology of the coast alter the amount of material reaching the deep fjords. Many deltas in Greenland provide essential ecosystem services and support the indigenous society[20]; a changing deltaic environment could ultimately alter not only their livelihoods[9] but also the archaeological evidence of the past[21]. How Greenland's coast responds to the changing climate remains unknown, and a general understanding of the processes causing delta changes in this vulnerable region has been largely absent. Arctic climate, including the climate in the Greenlandic region, has undergone striking changes in the past decades, much larger than observed elsewhere globally[22]. In some regions, the mean annual temperature has increased by more than 4° since 1979 (ref. 23), and the sea ice is breaking up earlier in the season[8] and refreezing later. This rapid warming results in more pronounced mass loss from the Greenland Ice Sheet and increasing freshwater runoff[14]. However, the effect of climate change in the Arctic coastal zone remains poorly documented and understood[9].

We analyse the depositional and erosional history of 121 Greenlandic deltas by mapping the majority (around 95%) of deltas along more than 3,000 km of Arctic coastline stretching from 70° N in West Greenland to 60° N in East Greenland (Supplementary Table 1). We use historical aerial imagery from the 1940s, aerial orthophotographs (that is,

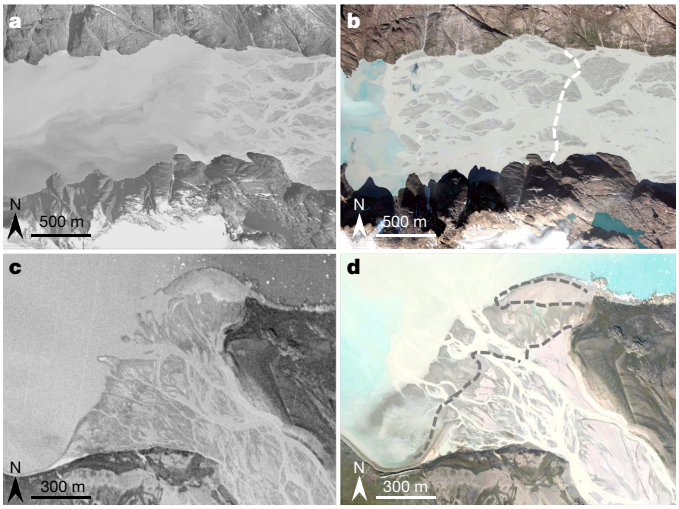

Figure 1 | Progradation in two types of deltas. a, **b**, 'Restricted delta' in 1985 (**a**, black and white orthophotograph) and 2010 (**b**, GEO1 satellite image, 20 August 2010). **c**, **d**, 'Open fan-shaped delta' in 1985 (**c**, black and white orthophotograph) and 2013 (**d**, WorldView-2 satellite image, 19 June 2013). The dashed lines in **b** (white) and **d** (grey) indicate the 1985 positions of the delta mouths. Both satellite images are provided by Google Earth.

[1]Center for Permafrost (CENPERM), University of Copenhagen, DK-1350 Copenhagen, Denmark. [2]Department of Biology, Freshwater Biology, University of Copenhagen, DK-2100 Copenhagen, Denmark. [3]Centre for GeoGenetics, Natural History Museum of Denmark, University of Copenhagen, DK-1350 Copenhagen, Denmark. [4]Department of Earth System Science, University of California Irvine, California 92697, USA. [5]NASA Jet Propulsion Laboratory, Pasadena, California 91109, USA. [6]Institute of Arctic and Alpine Research, University of Colorado, Boulder, Colorado 80309, USA. [7]Cooperative Institute for Research in Environmental Sciences and Department of Geological Sciences, University of Colorado, Boulder, Colorado 80309, USA. [8]DTU Space, National Space Institute, Technical University of Denmark, DK-2800 Lyngby, Denmark. [9]Geological Survey of Denmark and Greenland (GEUS), Glaciology, DK-1350 Copenhagen, Denmark. [10]Asiaq Greenland Survey, Postbox 1003, 3900 Nuuk, Greenland.
*These authors contributed equally to this work.

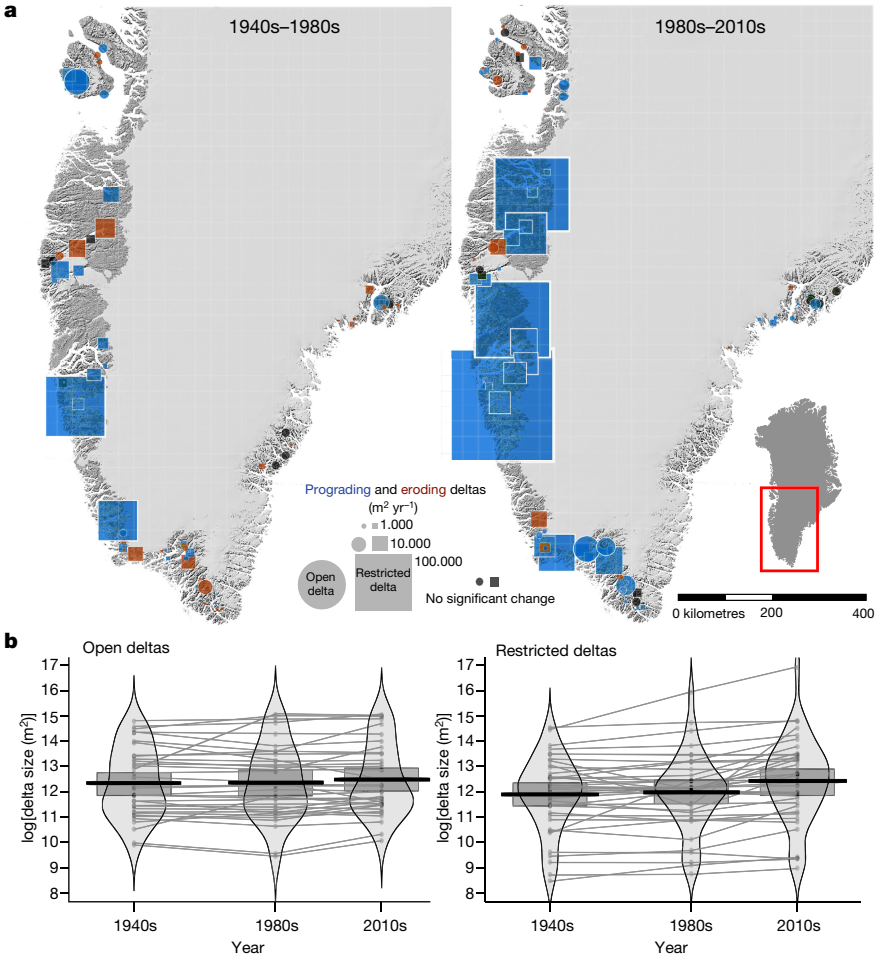

Figure 2 | Delta changes in the period between 1940s–1980s and 1980s–2010s. a, Blue dots or blue squares represent prograding deltas; red dots or red squares, eroding deltas. **b**, Density distributions (violin plots) of the delta sizes for each point in time (open deltas, $n = 35$; restricted deltas, $n = 40$). The central horizontal black line represents the mean, and the shaded boxes indicate the 95% highest density intervals of the mean. Individual deltas are marked by connecting lines between each plot. The average delta size is unchanged between the 1940s and 1980s on a log scale ($t = -0.78$, d.f. $= 148$, $P = 0.72$), whereas it significantly increases between the 1980s and 2010s ($t = -4.26$, d.f. $= 148$, $P < 0.001$).

geometrically corrected photographs, such that the scale is uniform) from the 1980s, and modern satellite imagery (2003–2016) available through Google Earth to analyse the spatial and temporal evolution of Greenlandic delta evolution (Methods; Supplementary Table 2). All the deltas can be classified as pristine systems; human interference (such as dykes and reservoir dams in the catchments, and coastal protection along the fringes) is non-existent. The areal extent of the selected deltas was measured at each observation time, and changes were determined as a change in square metres per year for two periods, 1940s–1980s and 1980s–2010s, with a persistent landward baseline used as a reference (Methods). The high-tide level marked the outer boundary of the delta (the delta front), and the tide level was estimated by using local tidal prediction tables (Methods). The presence of snow on the delta plain and of icebergs in the intertidal zone, together with the location of subaerial bars, aided the identification of delta areal extent (Methods; Extended Data Fig. 1). We introduce two different delta types, differentiated by their exposure to waves (Methods): a 'restricted delta' (Fig. 1a and b) is often located in the head of a fjord with waves coming from limited directions, in contrast to an 'open fan-shaped delta' (Fig. 1c and d), which experiences a potentially wide range of wave directions. The evolution of deltas is determined by competition between the influence of the terrestrial drainage basin and that of the marine receiving basin[24]. We hypothesize that the main terrestrial driver is spatial and temporal variation in freshwater runoff which controls sediment influx to the delta front, whereas the main marine driver is hypothesized to be the length of the open-water season and associated wave impact, which controls sediment erosion and reworking away from the delta front. To investigate the processes responsible for delta evolution, we analyse the direct and indirect effects of these terrestrial and marine drivers using structural equation modelling (SEM) (Methods; Extended Data Table 1). SEM consists of a meta-model (Extended Data Fig. 2) built on prior expected relationships between the runoff component of the glacial surface mass balance and runoff from land[25], local air temperatures[25], elastic and visco-elastic bedrock uplift[26], sea-ice coverage[8] and changes in delta areal extent (calculation of each driver is described in the Methods and Supplementary Information). The meta-model quantifies the proposed relationships and explores the potential missing linkages (Methods; Extended Data Tables 2 and 3).

Of the 121 deltas, observations of 75 cover the entire observational period (1940s, 1980s, and 2010s). Significant changes in average delta size have taken place for these deltas between the 1940s and 2010s (likelihood ratio test $= 27.23$, degrees of freedom (d.f.) $= 2$, $P < 0.001$; Fig. 2). Although there were no significant changes in average delta size in the early period, 1940s–1980s (t-value, $t = -0.78$, d.f. $= 148$, $P = 0.72$), there was an increase in delta size in the most recent period, 1980s–2010s ($t = -4.26$, d.f. $= 148$, $P < 0.001$). For the period 1980s–2010s, when delta progradation occurred, the changes in delta areal extent were positively correlated with increasing runoff when this coincided with open-water periods. High background freshwater runoff has developed large deltas, and the largest progradation rates are found in these deltas. Higher air temperatures affect the delta progradation

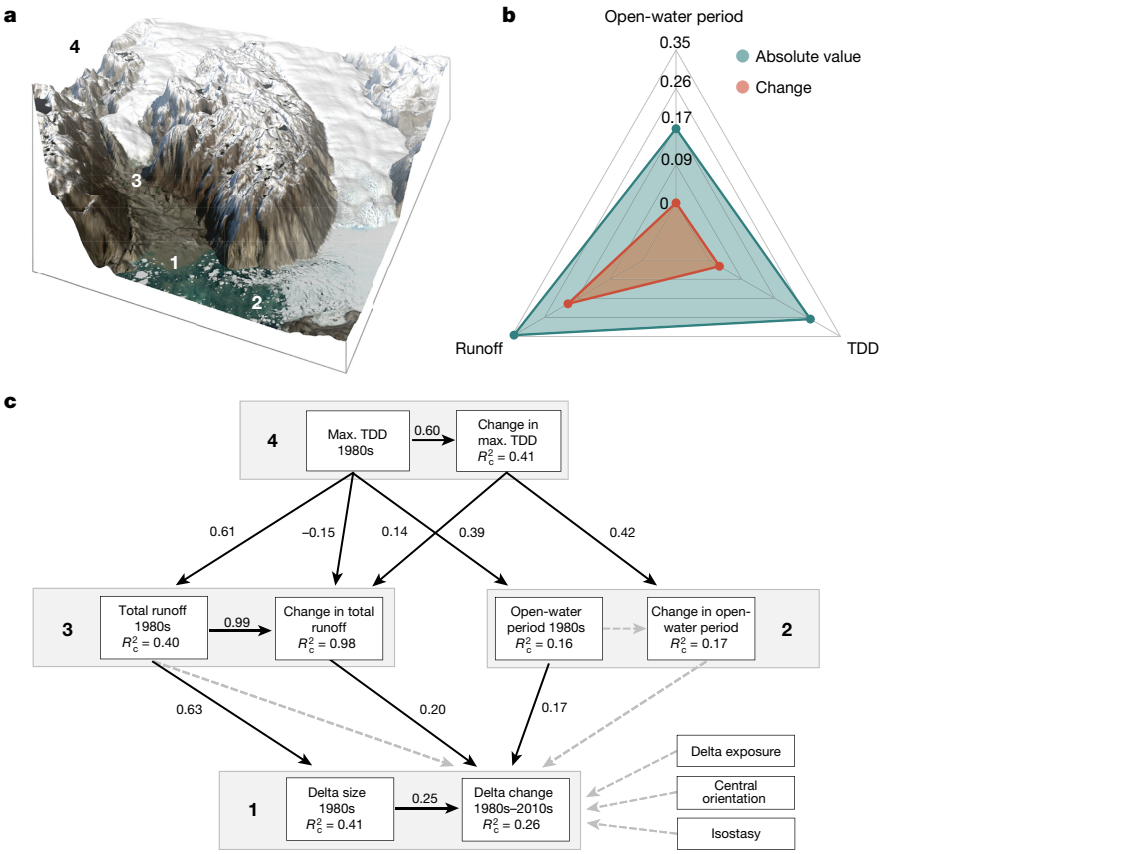

Figure 3 | Structural equation model representing connections between delta changes in a progradation period and factors influencing coastal evolution. a, Main terrestrial and marine drivers influencing delta changes incorporated in the SEM. The numbers refer to different sections in the SEM (see Methods). **b**, Total effect sizes on delta changes, from absolute values and changes in values of runoff, open-water period and thawing degree-days (TDD). Values represent the sum of potential pathways from each parameter to delta changes in the SEM. **c**, Solid arrows represent significant linear paths supported by the model; dashed lines are omitted paths. Model fit and path estimates are built on an SEM incorporating the random effect of delta types (restricted and open deltas). Fisher C statistic 28.3, with 30 model degrees of freedom and $P = 0.57$ (indicating close fit between model and data).

rate indirectly, both through increased runoff and associated increase in sedimentary flux, and by increasing the number of sea-ice-free days (Fig. 3a and c). The effect of increased meltwater dominates the delta response as compared with the effect of expanding sea-ice-free periods (Extended Data Fig. 3). The net effect of delta changes is governed by the initial environmental conditions at each delta in the 1980s rather than by relative changes in these conditions in the period between the 1980s and 2010s (Fig. 3b). This means that there is a clear trend in the spatial variation in delta changes (Fig. 2a): south and southwest Greenland show the most pronounced progradation in delta size, and deltas in central western Greenland have also prograded. In eastern Greenland, however, only a few deltas show minor progradation. The highest progradation rates are found in areas where both the 1980s runoff and the change in runoff over 1980s–2010s are high (Extended Data Fig. 4). The stable nature of deltas in East Greenland can be attributed to a combination of the generally lower temperatures, lower runoff, and the presence of sea-ice flux from the East Greenland Current (Extended Data Figs 4 and 5), which counteracts a local signal caused by sea-ice melting (Fig. 3c).

The regime of the deltas is governed by the freshwater runoff and associated sediment load from the catchment, and by the waves and tide from the receiving basin[27]. Here we show that delta progradation from 1980s to 2010s occurred after four decades of near-stability. The SEM analysis quantitatively attributes the recent progradation of deltas to an increasing freshwater runoff[13] and an increase in the open-water period during approximately the past 30 years (ref. 8). Our results show that sediment export dominates wave erosion, possibly because many deltas are located in protected environments and exposed to only limited wave energy: when these conditions are combined with the increasing sediment flux caused by higher freshwater runoff, the deltas prograde. We find a robust relation between progradation and increasing runoff which indicates uniform accommodation space (the space available for potential sediment accumulation) such that an increased sediment volume results in a proportionally increased progradation.

Arctic deltas are influenced by unique characteristics such as permafrost and changing seasonal water and ice conditions. They can generally be divided into two distinct types: large deltas (such as the Lena and Mackenzie River deltas) with large drainage basins, low gradients, strong seasonality in discharge, and strong variability of erosion and accretion patterns; and smaller deltas (Greenlandic deltas), with minor partly ice-covered drainage basins and steeper gradients, for which snow and ice melt control the runoff[28]. We studied the latter type and have shown that over the 1980s–2010s the pristine Greenlandic deltas prograded because of a warming climate which increases the freshwater runoff from the ice sheet and subsequent deposition at the nearby coast. Temperature, precipitation, and the area and mass balance of glacial ice within the delta catchment control the freshwater runoff potential (Fig. 3c and Extended Data Fig. 6) which causes the response signal in the deltas. The catchment size and the associated ice bodies vary for each delta investigated, and it is usually possible to distinguish whether an ice body is part of the Greenland Ice Sheet, peripheral glaciers or ice caps. The Greenland Ice Sheet already has the potential to deliver an ever-increasing supply of sediment and freshwater runoff, whereas peripheral glaciers and ice caps have a relatively limited ability to deliver sediment. Future changes in runoff and, by extension, the delta size are governed by the fate of the ice in the delta

catchment and the length of the open-water period. This prograding trend is likely to continue in the near future[29] and therefore be important for local society and stakeholders in the planning of infrastructure stability, not least because most of the Greenlandic population lives in or near the coast. The East Greenland deltas that are now stable may well overcome the threshold of sediment transport and start to become active prograding systems under a continuing warming trend. While the world's temperate deltas are drowning[30], Greenland's deltas are, in contrast, advancing because of the increased mass loss from Greenland's land-based ice. These Arctic deltas are a reminder of the influence of the sediment flux from land to sea; thus, the results presented here advance our understanding of processes controlling Arctic coastal evolution and their role in a future warmer climate.

Online Content Methods, along with any additional Extended Data display items and Source Data, are available in the online version of the paper; references unique to these sections appear only in the online paper.

Received 22 March; accepted 28 July 2017.

1. IPCC *Climate Change 2013: The Physical Science Basis* (eds Stocker, T. F. *et al.*) (Cambridge Univ. Press, 2013).
2. Jones, B. M. *et al.* Increase in the rate and uniformity of coastline erosion in Arctic Alaska. *Geophys. Res. Lett.* **36,** L03503 (2009).
3. Lantuit, H. *et al.* Coastal erosion dynamics on the permafrost-dominated Bykovsky Peninsula, north Siberia, 1951–2006. *Polar Res.* **30,** 7341 (2011).
4. Lantuit, H. & Pollard, W. H. Fifty years of coastal erosion and retrogressive thaw slump activity on Herschel Island, southern Beaufort Sea, Yukon Territory, Canada. *Geomorphology* **95,** 84–102 (2008).
5. Lantuit, H. *et al.* The Arctic Coastal Dynamics database: a new classification scheme and statistics on Arctic permafrost coastlines. *Estuaries Coasts* **35,** 383–400 (2012).
6. Rachold, V. *et al.* Coastal erosion vs riverine sediment discharge in the Arctic Shelf seas. *Int. J. Earth Sci.* **89,** 450–460 (2000).
7. Solomon, S. M. Spatial and temporal variability of shoreline change in the Beaufort–Mackenzie region, northwest territories, Canada. *Geo-Mar. Lett.* **25,** 127–137 (2005).
8. Barnhart, K. R., Miller, C. R., Overeem, I. & Kay, J. E. Mapping the future expansion of Arctic open water. *Nat. Clim. Change* **6,** 280–285 (2015).
9. Fritz, M., Vonk, J. E. & Lantuit, H. Collapsing Arctic coastlines. *Nat. Clim. Change* **7,** 6–7 (2017).
10. Overeem, I. *et al.* Sea ice loss enhances wave action at the Arctic coast. *Geophys. Res. Lett.* **38,** L17503 (2011).
11. Bhatt, U. S. *et al.* Implications of Arctic sea ice decline for the Earth system. *Annu. Rev. Environ. Resour.* **39,** 57–89 (2014).
12. Stroeve, J. C., Markus, T., Boisvert, L., Miller, J. & Barrett, A. Changes in Arctic melt season and implications for sea ice loss. *Geophys. Res. Lett.* **41,** 1216–1225 (2014).
13. Kjeldsen, K. K. *et al.* Spatial and temporal distribution of mass loss from the Greenland Ice Sheet since ad 1900. *Nature* **528,** 396–400 (2015).
14. van den Broeke, M. R. *et al.* On the recent contribution of the Greenland ice sheet to sea level change. *Cryosphere* **10,** 1933–1946 (2016).
15. de Winter, I. L., Storms, J. E. A. & Overeem, I. Numerical modeling of glacial sediment production and transport during deglaciation. *Geomorphology* **167–168,** 102–114 (2012).
16. Hawkings, J. *et al.* The Greenland Ice Sheet as a hot spot of phosphorus weathering and export in the Arctic. *Glob. Biogeochem. Cycles* **30,** 191–210 (2016).
17. Hawkings, J. R. *et al.* The effect of warming climate on nutrient and solute export from the Greenland Ice Sheet. *Geochem. Persp. Lett.* **1,** 94–104 (2015).
18. Pedersen, J. B. T. *et al.* Fluctuations of sediment accumulation rates in front of an Arctic delta in Greenland. *Holocene* **23,** 860–868 (2013).
19. Smith, R. W., Bianchi, T. S., Allison, M., Savage, C. & Galy, V. High rates of organic carbon burial in fjord sediments globally. *Nat. Geosci.* **8,** 450–453 (2015).
20. Forbes, D. L. *State of the Arctic Coast 2010: Scientific Review and Outlook* (Helmholtz-Zentrum Geesthacht, 2011).
21. Hollesen, J., Matthiesen, H., Moller, A. B. & Elberling, B. Permafrost thawing in organic Arctic soils accelerated by ground heat production. *Nat. Clim. Change* **5,** 574–578 (2015).
22. Serreze, M. C. & Barry, R. G. Processes and impacts of Arctic amplification: a research synthesis. *Global Planet. Change* **77,** 85–96 (2011).
23. Cohen, J. *et al.* Recent Arctic amplification and extreme mid-latitude weather. *Nat. Geosci.* **7,** 627–637 (2014).
24. Elliott, T. in *Sedimentary Environments and Facies* (ed. Reading, H. G.) Ch. 13, 113–154 (Blackwell Science, 1986).
25. Fettweis, X. *et al.* Estimating the Greenland ice sheet surface mass balance contribution to future sea level rise using the regional atmospheric climate model MAR. *Cryosphere* **7,** 469–489 (2013).
26. Khan, S. A. *et al.* Geodetic measurements reveal similarities between post-Last Glacial Maximum and present-day mass loss from the Greenland ice sheet. *Sci. Adv.* **2,** e1600931 (2016).
27. Bendixen, M. & Kroon, A. Conceptualizing delta forms and processes in Arctic coastal environments. *Earth Surf. Proc. Land* **42,** 1227–1237 (2017).
28. Forbes, D. L. & Hansom, J. D. *Treatise on Estuarine and Coastal Science* Vol. 3: *Estuarine and Coastal Geology and Geomorphology,* 245–283 (Elsevier, 2011
29. Meyssignac, B., Fettweis, X., Chevrier, R. & Spada, G. Regional sea level changes for the twentieth and the twenty-first centuries induced by the regional variability in Greenland Ice Sheet surface mass loss. *J. Clim.* **30,** 2011–2028 (2017).
30. Syvitski, J. P. M. *et al.* Sinking deltas due to human activities. *Nat. Geosci.* **2,** 681–686 (2009).

Supplementary Information is available in the online version of the paper.

Acknowledgements This study would not have been possible without the aid of the Danish Geodata Agency (GST), who gave us access to the historical aerial photographs. The modern satellite imagery was obtained through the freely available online database Google Earth. M.B., A.K., A.W.-N. and B.E. acknowledge financial support from the Danish National Research Foundation (CENPERM DNRF100). L.L.I. was funded by the Carlsberg Foundation (grant 0604-02230B). A.A.B. acknowledges support from the Danish Council for Independent Research, grant DFF-610800469, and from the Inge Lehmann Scholarship from the Royal Danish Academy of Science and Letters. I.O. received support from the US National Science Foundation (NSF) Office of Polar Programs (grant ARC-0909349) and INSTAAR. S.A.K. was funded by the Danish Council for Independent Research (grant DFF-4181-00126). K.R.B. acknowledges support from the Annenberg Public Policy Center and NSF SI2-SSI Award 1450409. J.A. acknowledges the ClimateBasis programme of the Greenland Ecosystem Monitoring system (www.g-e-m.dk) and Asiaq Greenland Survey. K.L. was supported by Asiaq Greenland Survey.

Author Contributions M.B. and L.L.I. designed the study, and, together with A.A.B., B.E. and A.K., framed the research questions. M.B. and A.A.B collected the data used in the photographic data analysis, and J.A. and K.L. assembled parts of this data. I.O. and K.R.B. analysed sea-ice data, A.W.-N. and J.E.B. analysed the data for the regional climate model, S.A.K. analysed isostasy data, and M.B. and L.L.I. analysed the data and wrote the manuscript with contributions and inputs from all authors.

Author Information Reprints and permissions information is available at www.nature.com/reprints. The authors declare no competing financial interests. Readers are welcome to comment on the online version of the paper. Publisher's note: Springer Nature remains neutral with regard to jurisdictional claims in published maps and institutional affiliations. Correspondence and requests for materials should be addressed to M.B. (mette.bendixen@ign.ku.dk).

Reviewer Information *Nature* thanks M. Fritz, W. Pollard and the other anonymous reviewer(s) for their contribution to the peer review of this work.

METHODS

Aerial and satellite imagery. Selection of coastal zone region in this study is dictated by the availability of 1940s aerial photographs from a rediscovered archive of imagery[31]. The images were taken during a photo campaign in the Second World War. Over the 1940s, many oblique aerial images were recorded along the coasts of Greenland, with a scale of 1:40.000. The precise dates and camera details of the '1943 flights' are no longer available, and it is unclear when the flights took place. The best estimate is that these photographs were recorded in the second half of the war. The film rolls were handed over to the Danish National Survey and Cadastre after the war, and here the registration cards at the archive associated with these flight lines have the year "1943" and "1943?" noted on them. Therefore, we assume that the imagery dates from 1943. Some images were taken during flight campaigns in 1949. All 1940s vertical photographs were scanned from the contact print at 600 dpi, resulting in a ground resolution of about 2 m. Delta changes between 1940s, 1980s and 2010s are derived from direct observations of spatial delta extent. About 80% of the deltas investigated are covered by the images from 1940s. Additionally, vertical aerial photographs from 1981 and 1985, covering the entire coastal zone, have been used in the analysis. For these photographs, all flights were conducted in summer, from late June to early August, from an altitude of 13.000 m at a scale of 1:150,000. The photographs were later scanned to a resolution of approximately 15 μm (corresponding to a ground resolution of about 2 m), using a photogrammetric scanner with a geometric error of 1–3 μm. The photographs are part of a larger collection of images covering the entire ice-free areas of Greenland from 1978 to 1987, processed at the Palaeoclimate-Quaternary Group of the Centre for Geogenetics, Natural History Museum of Denmark. The 1:150,000-scale photographs from 1981 and 1985 have been aero-triangulated to the GR96 reference system. The resulting ortho-mosaics have a ground resolution of 4 m. They constitute the 1981/1985 data used in this study and serve as the horizontal reference for rectification of all other imagery in this study. All satellite imagery was provided by DigitalGlobe, obtained through the freely available Google Earth, and exported as JPEG files at the highest possible resolution (4,800 × 3,252). The precise date for each image varies from delta to delta, but spans from 2003 to 2016 (Supplementary Table 2 lists the image acquisition date for each delta, along with information on satellite type, incidence angle, and specific scene ID). Where several satellite images were available, the newest imagery was chosen in order to analyse the longest possible time span within the most recent period of investigation. Exceptions were made if snowcover hindered the georectification of the image. For historical images, we accepted the acquisition time, as there was only a single image available for each period.

Ground control of the imagery and digitizing process. All imagery used in this study has been co-registered to the digital ortho-mosaics of 1981/1985 aerial photographs. Individual image rectifications were made for each individual delta before digitizing the delta front. The strategy used in the rectifying phase is to minimize horizontal error. Distortion of the images is minimized by rectifying the images on an individual delta basis with tie-point registration to the 1981/1985 ortho-mosaics. For this study, the strategy for rectifying the oblique images is to place a high number of tie points close to the delta front, encircling the area to be digitized. Rectification is done using a second- or a third-order polynomial transformation[32] for which at least 10 tie points are placed. This transformation, where many tie points are available, forces the tie points in the oblique image to the ground-truth tie points of the 1981/1985 ortho-mosaic and interpolates values between tie points using a polynomial transformation[32]. Residual root mean square (r.m.s.) value is no indication of an accurate rectification, but serves as an indicator of how much the image is distorted into its new position. The original resolution for the 1940s imagery was about 1.7 m resulting in a residual r.m.s. of maximum 10 m, while the modern satellite-derived imagery has original resolutions ranging from 0.3 to 0.8 m giving a residual r.m.s. of maximum 5 m. Once the images have been rectified to the 1981/1985 orthorectified mosaic, the delta area extent (A) is digitized manually, and the high-water line serves as boundary for the delta front. A reference line is drawn inland and constitutes the baseline for that delta throughout all investigated years. The result is a polygon representing the delta area extent for a specific time (A_i). When the delta area extent has been digitized for several years (t_i), each polygon is used to calculate change in delta area extent (in m^2):

$$dA = A_i - A_j \quad (1)$$

The period of change (in years) is given as:

$$dt = t_i - t_j \quad (2)$$

and the delta area extent change rate (P) is given as:

$$P = \frac{dA}{dt} \quad (3)$$

We narrow down the uncertainty of the horizontal accuracy to one pixel size (ρ), related to the 1981/1985 imagery and corresponding to 2 m. The uncertainty in the change rate of the delta area extent is given as:

$$\sqrt{2\rho^2} \quad (4)$$

The resulting uncertainty is 2.83 m.

Specific delta characteristics. The areal extent of each delta is identified at each time step. The high-water line on the delta plain was used as the delta shoreline. Identification of the high-water line was not always trivial, and we used additional measures. Icebergs and slush ice on the delta plain always indicated intertidal areas; snow and densely vegetated areas were only present on the subaerial delta plain above the high-water line. Subaerial bars on the delta plain were also incorporated in the areal extent of the delta. Delineation of the extent of the delta carries some subjectivity. To minimize this effect, the defined delta boundaries were verified by two or three people. Deltas were used only if two coastal morphologists could identify the same delta shoreline independent of each other. To address the uncertainties associated with categorizing the documented delta changes (prograding, eroding or stable), we divided the difference in delta area extent dA (in m^2) between the two periods by the total length of the delta front for both periods (in m). Absolute values greater than the estimated uncertainty of 2.83 m suggest an observed dA greater than could be produced by measurement errors alone.

For each delta, the maximum and minimum fetch length (the length of exposed water over which wind has blown) and direction were measured along with the open-angle width referred to as 'delta exposure' in the SEM analysis. The open-angle width is defined as the total angle (in degrees) for which the fetch exceeds 3 km. The 'central orientation' is given as the cross-shore normal angle minus the central total open-angle width (Supplementary Table 1). Both variables refer to a delta's exposure to wave energy.

In all analytical steps, we handled differences in delta dynamics caused by the differences between the two identified delta types, open and restricted deltas, as two randomly chosen instances interesting only as representatives of a common mean. This was done by including delta type as a random effect in the linear regression and structural equation model. Delta changes between the three studied time slices were described using a linear mixed effect model. For 75 deltas from which data on delta sizes in the 1940s, 1980s and 2010s could be retrieved, an initial linear model was created that included delta size as the response variable, period as the explanatory class variable, and delta ID and delta type as random effect variables. To meet the assumption of variance homogeneity in the model, delta size was log-transformed before any model reduction step. The reported P-value corresponds to a likelihood ratio-test. Within the random effect model, pairwise comparisons between the study periods (1940s versus 1980s, and 1980s versus 2010s) were based on differences in mean values. For each year, we used Satterthwaite approximations[33] to define the effective number of degrees of freedom used to estimate the 95% confidence limits around the mean. Based on these uncertainties, differences in mean values were tested via a two-tailed t-test. All P-values were evaluated at a 5% significance level.

Modelling delta changes. Our goal was to provide a framework that had the potential to clarify the impact of climate change on deltas in Greenland. Based on our knowledge from literature on dynamics influencing Arctic coastal evolution, we constructed a hypothetical meta-model that guided the further analysis (Extended Data Fig. 2). In this model, we specifically want to address three issues that arise when discussing the impact of climate change on coastal evolution[5]:

(1) The direct effect of runoff from the Greenland Ice Sheet and open-water days on delta evolution;

(2) The effect of local temperatures on delta evolution;

(3) The impact of the initial environmental conditions for each delta versus the changes in conditions affecting the delta evolution.

We postulate that sea ice protects a coast from erosion induced by waves and storm surge, meaning that a prolongation of the sea-ice-free period ought to lead to increasing erosion of the deltas[10]. We expect runoff to affect the sizes of the deltas, meaning that large runoff will deliver large amounts of bedload and suspended material enabling the deltas to prograde[17]. Local temperatures are thought to affect deltas indirectly in two opposing ways: (1) by warmer temperatures providing transport capacity to supply more material into the coastal zone through larger runoff from the GIS, and (2) by warmer temperatures decreasing the sea-ice extent, allowing a longer open-water period in which waves can affect the coast.

Sea-ice distribution. Satellite-derived estimates of the number of open-water days were calculated using the method of[8,34] using sea-ice concentration provided through the National Snow and Ice Data Center[35]. The data set covers the time period of late 1978 to the present at daily resolution and has a nominal horizontal resolution of 25 km. We restrict our analysis to the period from 1981/1985 to align with remotely sensed imagery intervals. For each grid cell and for each year, we

calculate the total number of open-water days, meaning the number of days when sea-ice concentration is less than 15%. The analysis period starts and ends at the 70th day of the year, to align the analysis year with the seasonal sea-ice maximum. The analysis is restricted to grid cells in which sea-ice concentration over a single day exceeded 80% at least once during the observational period.

Defining yearly isostatic uplift rates since the 1980s. For each location, we estimate uplift owing to a combination of the Earth's instantaneous elastic response to contemporary present-day changes in ice mass and delayed viscoelastic response to ice changes since the Last Glacial Maximum (approximately 21 thousand years ago) as described by ref. 26. To predict the elastic displacements, we convolve mass-loss estimates inferred from satellite and airborne altimetry data during 1995–2016 (from the ERS 1and 2 satellites, ICESat, the ATM and LVIS altimeters, and CryoSat-2) with the Green's function for vertical displacements derived[36] for the preliminary reference Earth model[37]. For dates before 1995, we convolve the mass loss inferred from surface mass balance (obtained using the regional climate model RACMO2)[38] with the Green's function for vertical displacements.

Delta catchment definition. Delta catchments were found by using a watershed analysis in Esri's ArcGIS software. A Greenland Mapping Project (GIMP) digital elevation model[39], with sinks filled, was used to create a flow direction and flow accumulation rasters. Points are placed for each delta, near the delta where major flow accumulation merges. For deltas where several flowlines exist, multiple points are placed. The catchments have been divided into ice-free land and glacier-covered land using the GIMP ice sheet mask[39] and the Randolph Glacier Inventory for local glaciers and ice caps[40].

Regional Climate Model MAR v.3.5.2 model. Runoff and air temperature data are acquired from the regional climate model MAR (Modèle Atmosphérique Régional) version 3.5.2 (ref. 41) from 1981/1985 to the present. The model is fully coupled with the CROCUS snow model, allowing for snow redistribution[41], and validated against the surface mass balance of the Greenland ice sheet, and parameterized as described in ref. 25. Here, we use the results from a model run from 1979 to 2014. The model data are forced with ERA-Interim reanalysis data, and topographically downscaled to a 5 km grid, based on ref. 42, in time steps of monthly means. Grid cells intercepting with the delta catchments were extracted, and weighted according to the coverage of each grid cell, relative to the total catchment area. Intercepting areas were derived using ArcMap 10.3 (Esri)[32]. Grid cells with a sea-mask sign were discarded. Thawing degree-days (TDD), which are a measure of both duration and magnitude of above-thawing temperatures during a specified period, were computed using the Climate Data Operators software (CDO, Max Planck Institute), as cumulative air temperatures above 0 °C per year. Runoff was computed as cumulative water equivalents per year (runoff (mm yr^{-1}) × area (km^2)). The maximum TDD and cumulative runoff were subsequently computed per catchment. Maximum TDD represents the single highest grid-cell value within each catchment. Trends (slopes) in all data variables are computed in CDO. They are based on linear ordinary least-square regressions of yearly averages to remove autocorrelation effects.

Structural equation modelling. To evaluate the effects of the selected environmental factors on delta change from the 1980s to 2010s, we used SEM. In SEM, causal links between variables of interest are defined and evaluated in the form of interconnected equations[43,44]. We created a hypothetical path diagram based on our expected connections between parameters (Extended Data Fig. 1). This meta-model was evaluated by a semi-explorative approach in which we included missing links and assessed the support of existing links using the data available[45]. Given the nature of each exogenous variable, we established causal inclusion rules that had to be met in order to include pathways suggested by the data. Variables describing a change from the 1980s to the 2010s could not affect initial variables in the 1980s. Furthermore, we did not consider paths indicating causal links from surface (delta sizes, sea ice and runoff) to the climate variables in the SEM. In the SEM, all endogenous variables were modelled using linear Gaussian mixed-effect models, containing delta type as a random intercept and the explanatory variables as fixed effects (Extended Data Table 1). Each local model was screened for residual distributional properties. Several variables were transformed as a result of evaluations in order to meet the assumptions of variable homogeneity in the local models (Extended Data Table 2). Model fit and model evaluation were based on local estimations, in which each path is solved independently from the others[46]. We evaluated the full SEM and potential inclusion of missing paths using Fisher's C statistic[47]. In contrast to global estimated models, local estimators permit complex path specifications fitted by the entire covariance matrix and do not transfer misspecification errors across different parts of a SEM[48]. In each of the local models, the links supported by our data were identified based on corrected Akaike Information Criteria (AICc)[49]. Based on all potential parameter combinations, the simplest model within two units of the lowest AICc value was included in the SEM (Extended Data Table 4). If one single model could not be identified, the model combining candidate models was used, on the condition that this combination provided a lower AICc. This fitting procedure was repeated until no further changes to the SEM could be made (Extended Data Table 3)[45]. In the final SEM, we controlled for error correlates between changes in maximum TDD and total runoff in 1980s and the open-water period in the 1980s, as these were suggested to cause changes in maximum TDD. Attempts to determine some simple general explanation for these links were not successful, so we regard these as background control features conditioned by an unobserved causality. The level of variance explained by each component model for all response variables was given as the conditional R^2 (or pseudo R^2) based on the variance of both the fixed and random effects[50]. To contrast the importance of the different model components, the effect sizes and accumulated effects (total effects) across the SEM were derived from path coefficients scaled to a mean of 0 and standard deviation of 1. All analyses were conducted in R version 3.1.0 or later (www.R-project.org). We used the R software platform (v.3.1.0 or later) and the piecewiseSEM[46], MuMin[51], lme4[52], lsmeans[53] and nlme packages[54] for our SEM and mixed-effect model analyses.

Data availability. We use historical aerial imagery from the 1940s to map the delta extent manually. Raw imagery is made available for research purposes by the Danish Geodata Agency, a part of the Danish Ministry of Energy, Utilities and Climate. The 1980s orthophotographs used in this study are available upon request from the corresponding author. Data on sea-ice concentration were provided by the National Snow and Ice Data Center (NSIDC) and are available through https://nsidc.org/data/nsidc-0051. The regional climate model MAR (Modèle Atmosphérique Régional) version 3.5.2 is available at ftp://ftp.climato.be/fettweis/MARv3.5/Greenland. Source data for Figs 2 and 3 are provided with the paper.

31. Bjørk, A. A. *et al.* An aerial view of 80 years of climate-related glacier fluctuations in southeast Greenland. *Nat. Geosci.* **5,** 427–432 (2012).
32. ArcGIS Desktop: Release 10. https://esri.com (Environmental Systems Research Institute, 2011).
33. Satterthwaite, F. E. An approximate distribution of estimates of variance components. *Biometrics* **2,** 110–114 (1946).
34. Barnhart, K. R., Overeem, I. & Anderson, R. S. The effect of changing sea ice on the physical vulnerability of Arctic coasts. *Cryosphere* **8,** 1777–1799 (2014).
35. Cavalieri, D., Parkinson, P., Gloersen, P. & Zwally, H. J. Sea ice concentrations from Nimbus-7 SMMR and DMSP SSM/I-SSMIS Passive Microwave Data, Version 1 (NASA National Snow and Ice Data Center Distributed Active Archive Center, 1996); accessed April 2016.
36. Petrov, L. & Boy, J. P. Study of the atmospheric pressure loading signal in very long baseline interferometry observations. *J. Geophys. Res. Solid Earth* **109,** B03405 (2004).
37. Dziewonski, A. M. & Anderson, D. L. Preliminary reference Earth model. *Phys. Earth Planet. Inter.* **25,** 297–356 (1981).
38. Ettema, J. *et al.* Climate of the Greenland ice sheet using a high-resolution climate model. Part 1: Evaluation. *Cryosphere* **4,** 511–527 (2010).
39. Howat, I. M., Negrete, A. & Smith, B. E. The Greenland Ice Mapping Project (GIMP) land classification and surface elevation data sets. *Cryosphere* **8,** 1509–1518 (2014).
40. Rastner, P. *et al.* The first complete inventory of the local glaciers and ice caps on Greenland. *Cryosphere* **6,** 1483–1495 (2012).
41. Brun, E., David, P., Sudul, M. & Brunot, G. A numerical model to simulate snow-cover stratigraphy for operational avalanche forecasting. *J. Glaciol.* **38,** 13–22 (1992).
42. Bamber, J. L., Layberry, R. L. & Gogineni, S. P. A new ice thickness and bed data set for the Greenland ice sheet. 1. Measurement, data reduction, and errors. *J. Geophys. Res. D* **106,** 33773–33780 (2001).
43. Shipley, B. Confirmatory path analysis in a generalized multilevel context. *Ecology* **90,** 363–368 (2009).
44. Grace, J. B. *Structural Equation Modeling and Natural Systems* (Cambridge Univ. Press, 2006).
45. Grace, J. B. *et al.* Guidelines for a graph-theoretic implementation of structural equation modeling. *Ecosphere* **3,** art73 (2012).
46. Lefcheck, J. S. piecewiseSEM: piecewise structural equation modelling in R for ecology, evolution, and systematics. *Methods Ecol. Evol.* **7,** 573–579 (2015).
47. Shipley, B. A new inferential test for path models based on directed acyclic graphs. *Struct. Equ. Modeling* **7,** 206–218 (2000).
48. Bollen, K. A., Kirby, J. B., Curran, P. J., Paxton, P. M. & Chen, F. Latent variable models under misspecification: two-stage least squares (2SLS) and maximum likelihood (ML) estimators. *Sociol. Methods Res.* **36,** 48–86 (2007).
49. Burnham, K. P. & Anderson, D. R. *Model Selection and Multimodel Inference: A Practical Information-Theoretic Approach* (Springer Science & Business Media, 2002).
50. Nakagawa, S. & Schielzeth, H. A general and simple method for obtaining R^2 from generalized linear mixed-effects models. *Methods Ecol. Evol.* **4,** 133–142 (2013).
51. Barton, K. MuMIn: Multi-Model Inference. R package version 1.15.6; https://CRAN.R-project.org/package=MuMIn (2016).
52. Bates, D., Maechler, M., Bolker, B. & Walker, S. lme4: linear mixed-effects models using 'Eigen' and S4. R package version 1.1-13; https://CRAN.R-project.org/package=lme4 (2014).
53. Lenth, R. V. Least-squares means: the R package lsmeans. *J. Stat. Softw.* **69,** 1–33 (2016).
54. Pinheiro, J. & Bates, D. DebRoy, S. & Sarkar, D. nlme: linear and nonlinear mixed effects models. R package version 3.1-117; http://CRAN.R-project.org/package=nlme (2014).

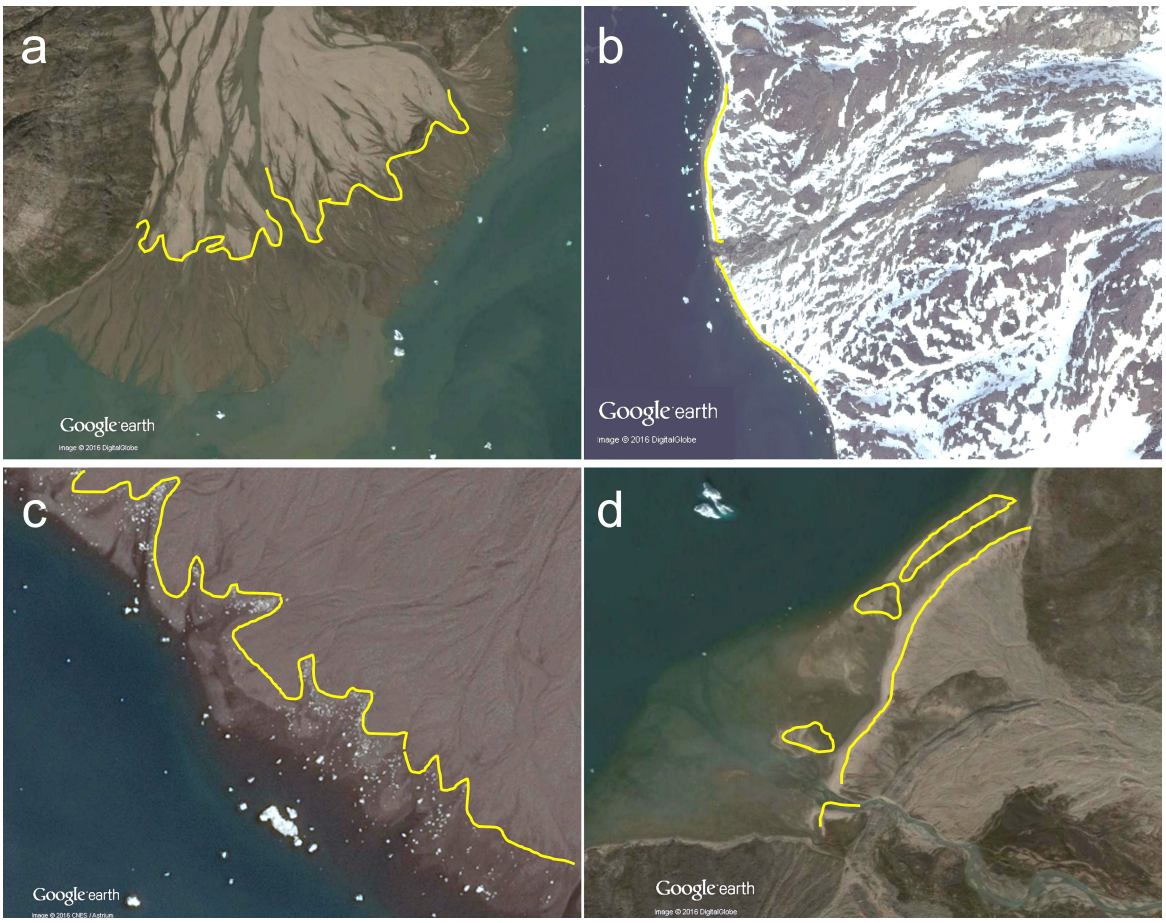

Extended Data Figure 1 | Examples of the identification of the delta extent. The land–water boundary is drawn where the high-water line (**a**) can be identified. Presence of snowcover (**b**) or icebergs (**c**) aids the identification process. Mouth bars (**d**) are included as part of the delta extent. All imagery provided by Google Earth.

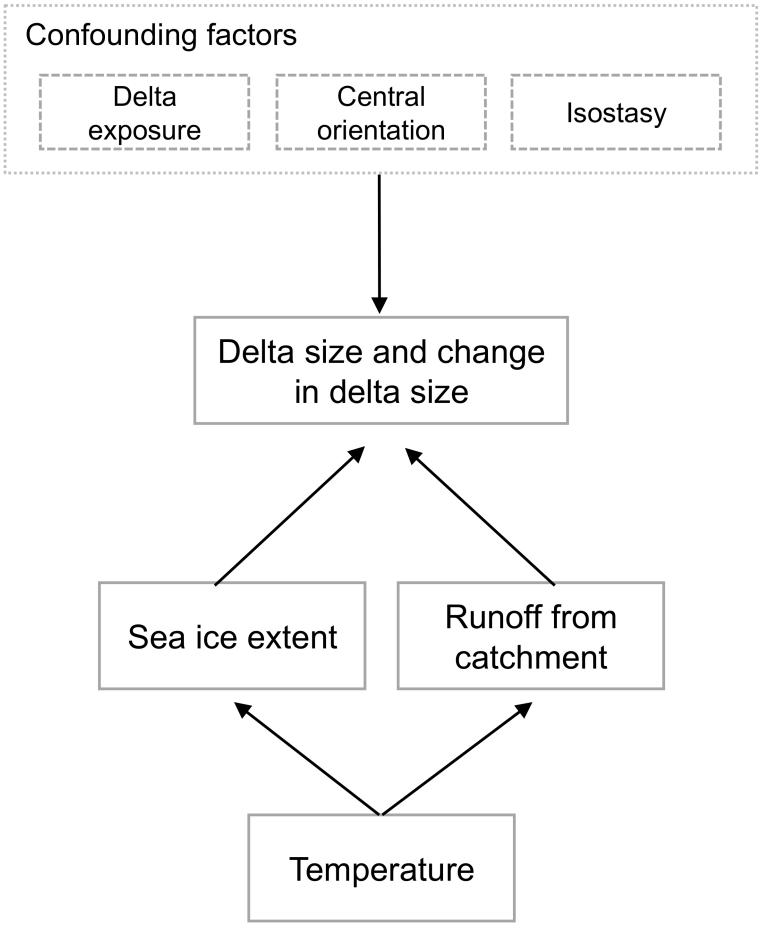

Extended Data Figure 2 | Meta-model showing hypothesized causal links from which a structural equation model was constructed. Justification and argumentation of each path is given in the main text and Methods section. Solid boxes indicate factors from which two options for each variable were constructed, one representing initial values in the 1980s and one representing changes from 1980s to the 2010s. Dashed boxes indicate variables that were expected to have a confounding effect on delta changes, potentially obscuring our target hypotheses.

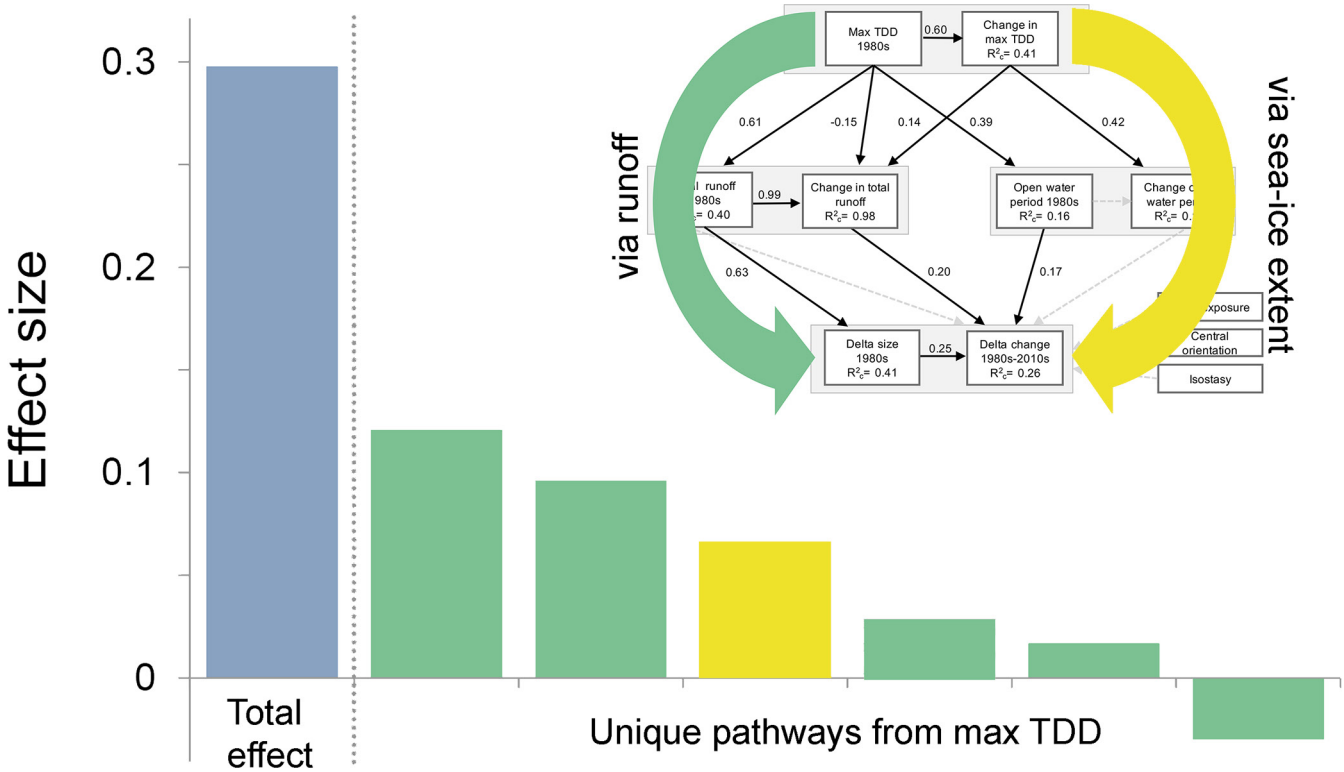

Extended Data Figure 3 | Total effect of TDD on delta changes derived from the SEM. The top-right insert indicates the direction of the pathways from TDD to delta changes in the structural equation model presented in Fig. 3. Green bars represent unique pathways via runoff; yellow bars represent unique pathways via sea-ice extent.

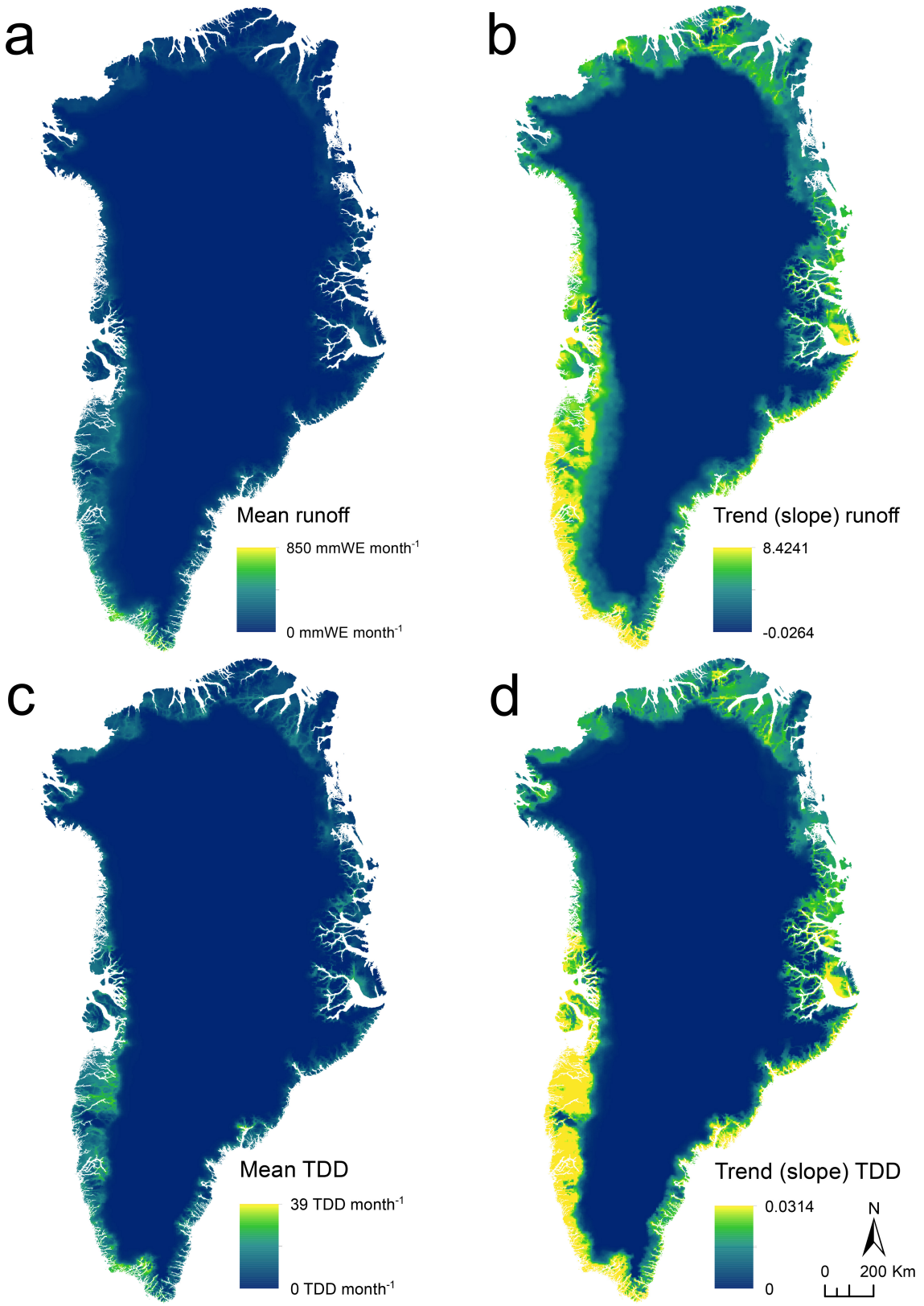

Extended Data Figure 4 | Spatial distribution of runoff and thawing degree days (TDD). a, Mean runoff; **b**, yearly change in runoff 1981–2014; **c**, mean TDD; **d**, yearly change in TDD from 1981–2014.

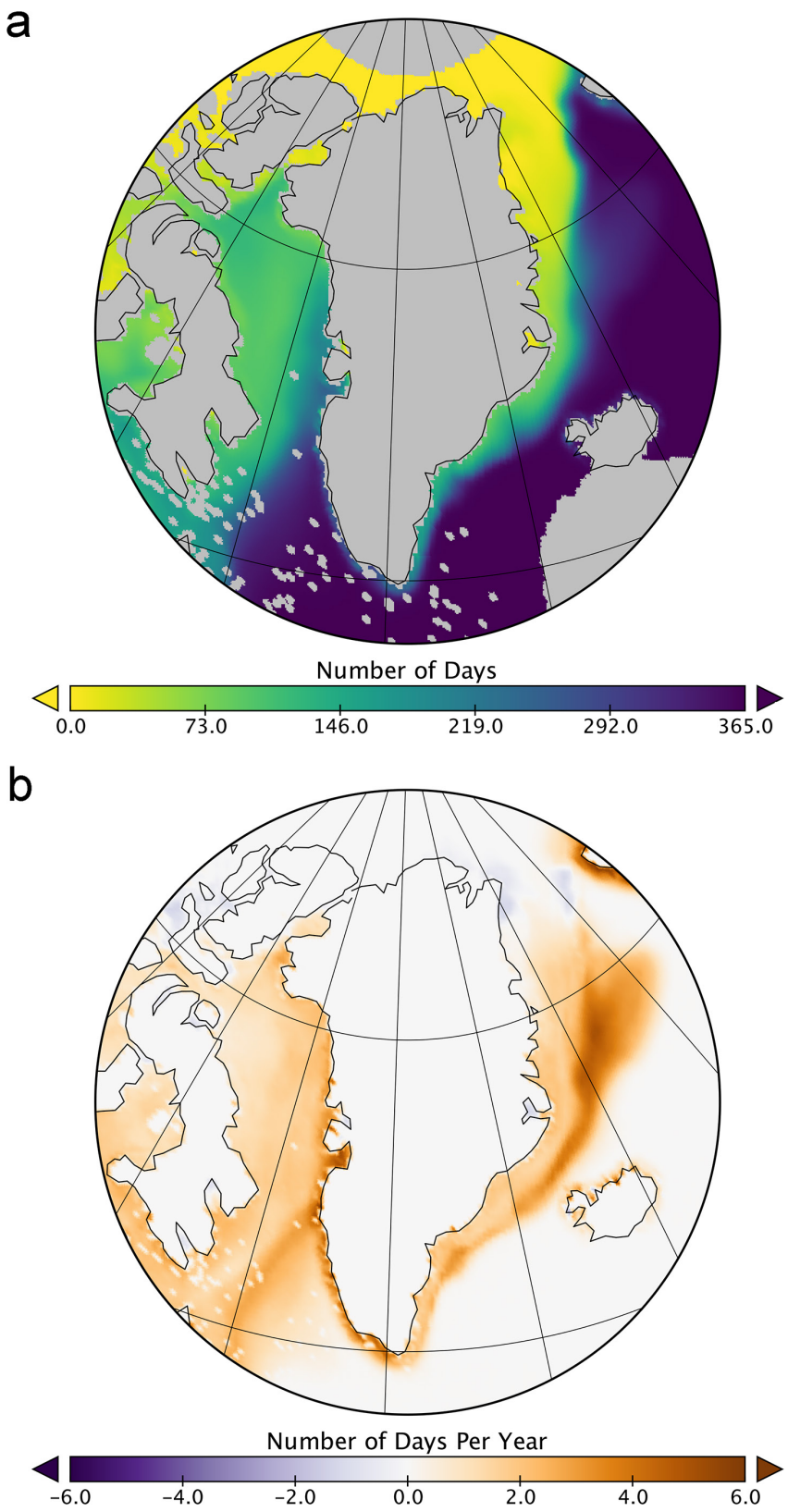

Extended Data Figure 5 | Spatial distribution of open-water days . **a**, Mean number of open-water days; **b**, yearly change in open-water days from 1981 to 2014.

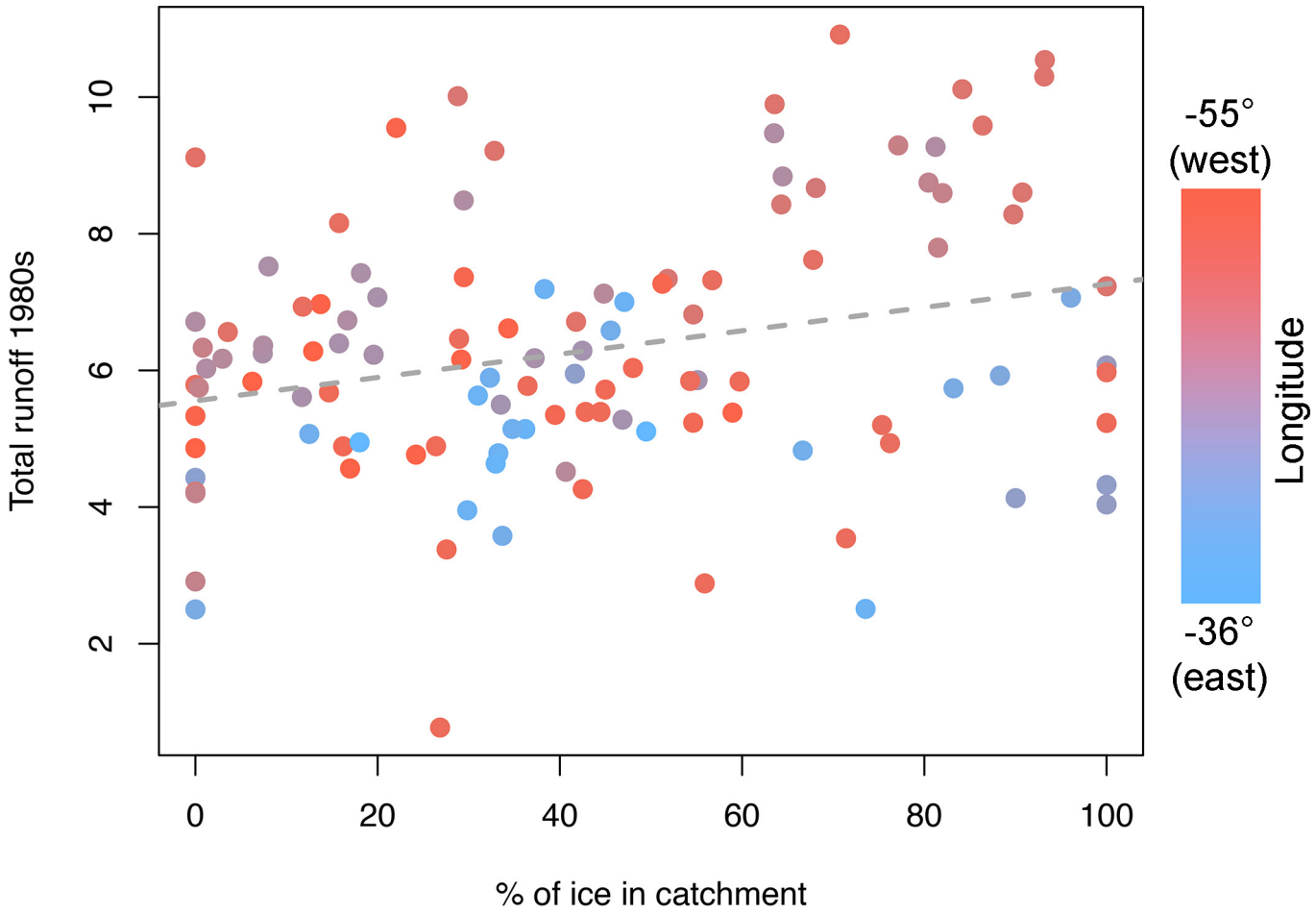

Extended Data Figure 6 | Total runoff from the studied delta catchments as a function of the ice coverage in the catchments. The dotted line indicates mean trend from 0% to 100% ice coverage. There is a significant linear increase in the log total runoff in the 1980s when the percentage of ice bodies in the catchment increases: slope estimate $\beta = 0.017$ [0.006; 0.028], (mean [95% confidence limits]), $P < 0.01$.

Extended Data Table 1 | Model variables

Model Variables*	Units
Delta size 1980s (log)	m^2
Delta change 1980s-2010s (cube root)	m2
Central orientation	Degrees
Delta exposure	Degrees
Isostasy	m^{-1} y^{-1}
Open water period 1980s	days
Change in open water period 1980s-2010s	days
Total runoff 1980s (log)	mmWE/month
Change in total runoff 1980s-2010s (log)	mmWE/month
Max TDD	days
Change in max TDD	days

*Data transformation given in brackets.

Extended Data Table 2 | Standardized partial effect sizes (and standard errors) and proposed interpretations

Response	Predictor	Magnitude	Standard error	Proposed interpretation
Delta change 1980s-2010s	Delta size 1980s	0.25	0.11	Large deltas change at a greater rate compared to their smaller counterparts
Delta change 1980s-2010s	Open water period 1980s	0.17	0.09	Reduced ice cover accelerates coastal changes
Delta change 1980s-2010s	Change in total run off	0.20	0.11	The bigger change in runoff, the greater are the changes in delta size
Delta size 1980s	Total run off 1980s	0.63	0.07	Large deltas are located in areas with high runoff
Open water period 1980s	Max TDD 1980s	0.39	0.09	Local high temperatures lead to longer periods with open water
Change open water period	Change in max TDD	0.42	0.09	Increases in local temperatures prolongs the open water period
Total run off 1980s	Max TDD 1980s	0.63	0.07	Local warm areas have the highest rates of run off
Change in total run off	Total run off 1980s	0.99	0.02	Areas with high rates of runoffs are also areas with the greatest gain in runoff
Change in total run off	Max TDD 1980s	-0.15	0.02	When accounting for the effect of runoff, the relative change in runoff is highest in local cold areas
Change in total run off	Change in max TDD	0.14	0.02	In areas were TDD increases, the runoff also increases
Change in max TDD	Max TDD 1980s	0.60	0.07	Locally warm areas are also the ones getting warmer

Extended Data Table 3 | Individual paths not included in the final structural equation

Path	Parameter estimate	Standard error	df	t-value	P-value
Delta change 1980s-2010s ~ Max TDD 1980s + ...	-0.10	0.26	110	-0.40	0.69
Delta size 1980s ~ Max TDD 1980s + ...	-0.02	0.03	112	-0.72	0.48
Change open water period ~ Max TDD 1980s + ...	-0.02	0.02	112	-0.78	0.44
Total runoff 1980s ~ Open water period 1980s + ...	0.00	0.00	112	0.82	0.41
Delta size 1980s ~ Open water period 1980s + ...	0.00	0.00	111	-0.35	0.73
Change in total runoff ~ Open water period 1980s + ...	0.00	0.00	110	1.10	0.28
Change open water period ~ Open water period 1980s+ ...	0.00	0.00	111	1.54	0.13
Delta change 1980s-2010s ~ Total runoff 1980s + ...	0.89	4.19	109	0.21	0.83
Change open water period ~ Total runoff 1980s + ...	0.04	0.09	111	0.42	0.67
Delta change 1980s-2010s ~ Change in max TDD + ...	407.32	309.33	109	1.32	0.19
Delta size 1980s ~ Change in max TDD + ...	29.24	28.00	111	1.04	0.30
Change open water period ~ Delta change 1980s-2010s+ ...	-0.01	0.01	109	-0.74	0.46
Change in total runoff ~ Delta size 1980s + ...	0.01	0.02	110	0.65	0.52
Change open water period ~ Delta size 1980s + ...	0.15	0.09	111	1.69	0.09
Change open water period ~ Change in total runoff +...	-0.12	0.42	110	-0.30	0.77

Endogenous variables are presented on the left side and the causal variable on the right side of the ~ mark. Conditional variables in each sub-model have been omitted from output table for clarity. Unstandardized parameter estimates are given along with their standard errors, degrees of freedom (df), *t*-values and associated probabilities.

Extended Data Table 4 | AICc values of local submodels derived from the initial meta model

Endogene variable		Explanatory parameters								df	logLik	AICc	ΔAICc
Delta change 1980s-2010s		Intercept	Delta exposure	Isostasy	Delta size 1980s	Change in total runoff	Total runoff 1980s	Central orientation	Open water period 1980s	Change open water period				
		-29.43			2.434	1.584		-0.043	0.027		7	-468.39	951.8	0
	*	-30.66			2.237	1.598			0.029		6	-469.75	952.3	0.44
		-37.39			2.523		1.490	-0.040	0.029		7	-468.72	952.5	0.66
		-38.32			2.279		1.606		0.030		6	-469.88	952.5	0.71
		-22.91			2.398	2.029		-0.047			6	-469.95	952.7	0.85
		-41.89			3.488			-0.044	0.035		6	-470.03	952.8	1.01
		-43.34			3.304				0.038		5	-471.40	953.3	1.51
		-21.13		-0.015	2.431	1.880		-0.049			7	-469.34	953.7	1.9
		-32.80			2.513		1.941	-0.044			6	-470.49	953.8	1.93
		-23.50			2.166	2.089					5	-471.61	953.8	1.94
		-21.14			2.499	3.388	-1.956	-0.047	0.026		8	-468.25	953.8	2.02
Delta size 1980s		Intercept	Total runoff 1980s	Open water period 1980s										
	*	9.26	0.598								4	-201.30	411	0
		9.38	0.611	-0.001							5	-201.16	412.9	1.91
		12.22		0.003							4	-229.76	467.9	56.93
Open water period 1980s		Intercept	1980s											
	*	127.70	5.56								4	-677.92	1364.2	0
		245.70									3	-687.66	1381.5	17.34
Change open water period		Intercept	Change in max TDD	Open water period 1980s										
	*	0.47	99.14								4	-198.56	405.5	0
		0.25	88.41	0.002							5	-197.67	405.9	0.4
		1.90		0.004							4	-205.54	419.4	13.96
Total runoff 1980s		Intercept	1980s											
	*	2.34	0.1862								4	-208.21	424.8	0
		6.29									3	-237.98	482.2	57.39
Change in total runoff		Intercept	Total runoff 1980s	Max TDD 1980s	Change in max TDD									
	*	-4.73	1.055	-0.05	45.15						6	-26.30	65.4	0
		-4.27	1.103	-0.03							5	-47.50	105.5	40.17
Change in max TDD		Intercept	1980s											
	*	0.01	0.0006								4	454.34	-900.3	0
		0.02									3	426.94	-847.7	52.65

Models within two AICc units of the sub-model with the lowest AICc value. Unstandardized parameter estimates are shown for each local model. Standardized parameter estimates derived from the unstandardized ones are presented in Fig. 3 and Extended Data Table 2. Each submodel is presented together with its degrees of freedom (df), log-likelihood estimate (LogLik), corrected Akaike Information Criteria value (AICc) and difference in AICc compared to the submodel with the lowest AICc (ΔAICc).
*Local models used in the final SEM.